

# A simple and robust method for automated photometric classification of supernovae using neural networks

N.V. Karpenka<sup>1\*</sup>, F. Feroz<sup>2</sup> and M.P. Hobson<sup>2</sup>

<sup>1</sup>The Oskar Klein Centre for Cosmoparticle Physics, Department of Physics, Stockholm University, AlbaNova, SE-106 91 Stockholm, Sweden

<sup>2</sup>Astrophysics Group, Cavendish Laboratory, J.J. Thomson Avenue, Cambridge CB3 0HE, UK

Accepted 2012 November 14. Received 2012 October 11; in original form 2012 August 7

## ABSTRACT

A method is presented for automated photometric classification of supernovae (SNe) as Type-Ia or non-Ia. A two-step approach is adopted in which: (i) the SN lightcurve flux measurements in each observing filter are fitted separately to an analytical parameterised function that is sufficiently flexible to accommodate virtually all types of SNe; and (ii) the fitted function parameters and their associated uncertainties, along with the number of flux measurements, the maximum-likelihood value of the fit and Bayesian evidence for the model, are used as the input feature vector to a classification neural network (NN) that outputs the probability that the SN under consideration is of Type-Ia. The method is trained and tested using data released following the SuperNova Photometric Classification Challenge (SNPCC), consisting of lightcurves for 21,319 SNe in total. We consider several random divisions of the data into training and testing sets: for instance, for our sample  $\mathcal{D}_1$  ( $\mathcal{D}_4$ ), a total of 10 (40) per cent of the data are involved in training the algorithm and the remainder used for blind testing of the resulting classifier; we make no selection cuts. Assigning a canonical threshold probability of  $p_{\text{th}} = 0.5$  on the network output to class a SN as Type-Ia, for the sample  $\mathcal{D}_1$  ( $\mathcal{D}_4$ ) we obtain a completeness of 0.78 (0.82), purity of 0.77 (0.82), and SNPCC figure-of-merit of 0.41 (0.50). Including the SN host-galaxy redshift and its uncertainty as additional inputs to the classification network results in a modest 5–10 per cent increase in these values. We find that the quality of the classification does not vary significantly with SN redshift. Moreover, our probabilistic classification method allows one to calculate the expected completeness, purity and figure-of-merit (or other measures of classification quality) as a function of the threshold probability  $p_{\text{th}}$ , without knowing the true classes of the SNe in the testing sample, as is the case in the classification of real SNe data. The method may thus be improved further by optimising  $p_{\text{th}}$  and can easily be extended to divide non-Ia SNe into their different classes.

**Key words:** methods: data analysis – methods: statistical – supernovae: general

## 1 INTRODUCTION

Much interest in supernovae (SNe) over the last decade has been focused on Type-Ia (SNIa) for their use as ‘standardizable’ candles in constraining cosmological models. Indeed, observations of SNIa led to the discovery of the accelerated expansion of the universe (Riess et al. 1998; Perlmutter et al. 1999), which is usually interpreted as evidence for the existence of an exotic dark energy component. Ongoing observations of large samples of SNIa are being used to improve the measurement of luminosity distance as a function of redshift, and thereby constrain cosmological parameters further (e.g., Kessler et al. 2009; Benitez-Herrera et al. 2012; Sullivan et al. 2011; Conley et al. 2011; March et al. 2011) and improve our knowledge of dark energy (e.g., Mantz et al.

2010; Blake et al. 2011). Moreover, the gravitational lensing of SNIa by foreground cosmic structure along their lines-of-sight has been used to constrain cosmological parameters (Metcalf 1999, Dodelson & Vallinotto 2006, Zentner & Bhattacharya 2009) and the properties of the lensing matter (Rauch 1991, Metcalf & Silk 1999, Jönsson et al. 2007, Kronborg et al. 2010, Jönsson et al. 2010a, Jönsson et al. 2010b, Karpenka et al. 2012). In addition to their central role in cosmology, the astrophysics of SNIa is also of interest in its own right, and much progress has been made in understanding these objects in recent years (e.g. Hillebrandt & Niemeyer 2000).

Other types of SNe are also of cosmological interest. Type II Plateau Supernovae (SNII-P), for example, can also be used as distance indicators, although only for smaller distances and to lower accuracy than SNIa. Compared to SNIa, however, for which there is still uncertainty regarding the progenitor system, SNII-P explo-

\* E-mail: nkarpenka@fysik.su.se

sions are better understood. Furthermore, since SNII-P have only been found in late-type galaxies, biases from environmental effects will most probably have a smaller effect on distance measurements using SNII-P. Thus, the differences between the two types of SNe will result in different systematic effects, allowing SNII-P data to complement SNIa analyses (D’Andrea et al. 2010).

Although not used directly in cosmology, other classes of SNe are a potential source of contamination when attempting to compile SNIa catalogues, most notably SN Ib/c. The consequences of such contamination have been considered by Homeier (2005). SN Ib/c are also of considerable astrophysical interest, in particular the nature of their progenitors (Fryer et al. 2007).

The next generation of survey telescopes, such as the Dark Energy Survey (DES; Wester & Dark Energy Survey Collaboration 2005, Annis et al. 2011), the Large Synoptic Survey Telescope (LSST; Tyson 2002, Ivezić et al. 2008), and SkyMapper (Schmidt et al. 2005), are expected to observe lightcurves for many thousands of SNe, far surpassing the resources available to confirm the type of each of them spectroscopically. Hence, in order to take advantage of this large amount of SNe data, it is necessary to develop methods that can accurately and automatically classify many SNe based only on their photometric light curves.

In response to this need, many techniques targeted at SNe photometric classification have been developed, mostly based on some form of template fitting (Poznanski et al. 2002; Johnson & Crots 2006; Sullivan et al. 2006; Poznanski et al. 2007; Kuznetsova & Connolly 2007; Kunz et al. 2007; Sako et al. 2008; Sako et al. 2011; Rodney & Tonry 2009; Gong et al. 2010; Falck et al. 2010). In such methods, the lightcurves in different filters for the SN under consideration are compared with those from SNe whose types are well established. Usually, composite templates are constructed for each class, using the observed lightcurves of a number of well-studied, high signal-to-noise SNe (see Nugent et al. 2002), or spectral energy distribution models of SNe. Such methods can produce good results, but the final classification rates are very sensitive to the characteristics of the templates used.

To address this difficulty, Newling et al. (2011) instead fit a parametrised function to the SN lightcurves. These post-processed data are then used in either a kernel density estimation method or a ‘boosting’ machine learning algorithm to assign a probability to each classification output, rather than simply assigning a specific SN type. More recently, Richards et al. (2012) and Ishida & de Souza (2012) have introduced methods for SN photometric classification that do not rely on any form of template fitting, but instead employ a mixture of dimensional reduction of the SNe data coupled with a machine learning algorithm. Richards et al. (2012) proposed a method that uses semi-supervised learning on a database of SNe: as a first step they use all of the lightcurves in the database simultaneously to estimate a low-dimensional representation of each SN, and then they employ a set of spectroscopically confirmed examples to build a classification model in this reduced space, which is subsequently used to estimate the type of each unknown SN. Subsequently, Ishida & de Souza (2012) proposed the use of Kernel Principal Component Analysis as a tool to find a suitable low-dimensional representation of SNe lightcurves. In constructing this representation, only a spectroscopically confirmed sample of SNe is used. Each unlabeled lightcurve is then projected into this space and a  $k$ -nearest neighbour algorithm performs the classification.

In this paper, we present a new method for performing SN classification that also does not rely on template fitting in a conventional sense, but combines parametrised functional fitting of the

SN lightcurves together with a machine learning algorithm. Our method is very straightforward, and might reasonably even be described as naive, but nonetheless yields accurate and robust classifications.

The outline of this paper is as follows. In Sec. 2, we describe the data set used for training and testing in our analysis, and we present a detailed account of our methodology in Sec. 3. We test the performance of our approach in Sec. 4 by applying to the data and present our results. Finally, we conclude in Sec. 5.

## 2 POST-SNPCC SIMULATED DATA SET

The data set we will use for training and testing our classification algorithm described below is that released by the Super-Nova Photometric Classification Challenge (SNPCC), which consists of simulations of lightcurves in several filters for 21,319 SNe (Kessler et al. 2010). The simulations were made using the SNANA package (Kessler et al. 2009) according to DES specifications. We used the updated version of the simulated data-set (post-SNPCC), which was made public after the challenge results were released. This updated data-set is quite different from the one used in the challenge itself, owing to some bug fixes and other improvements aimed at a more realistic simulation of the data expected for DES. The data set contains SNe of Types Ia, Ib/c, Ib, Ic, IIn, II-P and II-L, sampled randomly with proportions given by their expected rates as a function of redshift. Averaged over all redshifts, the approximate proportions of each type are 25, 1, 7, 5, 9, 51 and 2 per cent, respectively.

This large data set, which we denote by  $\mathcal{D}$ , is made up of two simulated subsamples: a small ‘spectroscopically-confirmed’ sample of 1,103 SNe, which we denote by  $\mathcal{S}$ , and a ‘photometric’ sample of 20,216 SNe, denoted by  $\mathcal{P}$ . The  $\mathcal{S}$  subsample consists of simulated lightcurves for a set of SNe that one could follow-up with a fixed amount of spectroscopic resources on each of a 4-m and 8-m class telescope. The magnitude limits were assumed to be 21.5 ( $r$  band) for the 4-m and 23.5 ( $i$  band) for the 8-m telescope. Since spectroscopy is more demanding than photometry,  $\mathcal{S}$  consists of SNe that on average have higher observed brightnesses and much lower host-galaxy redshifts than those in the photometric sample  $\mathcal{P}$ . Consequently,  $\mathcal{S}$  is not a random subset of  $\mathcal{D}$ , but instead has a much higher fraction of SNIa.

For each one of the SNe in  $\mathcal{D}$ , we denote the data by  $\mathbf{D}_i = \{t_{i,k}^\alpha, F_{i,k}^\alpha, \sigma_{i,k}^\alpha\}$ , where  $i$  indexes the SNe,  $\alpha \in \{g, r, i, z\}$  denotes the filter,  $k = 1, 2, \dots, n_i^\alpha$  indexes the number of flux measurements in filter  $\alpha$ ,  $t_{i,k}^\alpha$  is the time for the given measurements,  $F_{i,k}^\alpha$  is the SNANA ‘calibrated’ flux measured at time  $t_{i,k}^\alpha$  and  $\sigma_{i,k}^\alpha$  is the corresponding uncertainty. The lightcurve in each filter for each SN is measured on an irregular time grid that differs from filter to filter and between SNe. For each SN, between 16 to 160 measurements were made (between 4 and 40 measurements in each filter), with a median value of 101 measurements. We note that some of the SNe lightcurves were observed only before or after the peak in emission, but were still included in our analysis.

## 3 ANALYSIS METHODOLOGY

In order to perform the SNe classification, we adopt a two-step process:

- (i) SNe lightcurves are first fitted to an analytical parameterised

function, in order to standardise the number of input parameters for each SNe that are used in NN training. Provided that the function is flexible enough to fit important features in typical SN lightcurves, but sufficiently restrictive not to allow unreasonable fitted lightcurves, the resulting representation of the data reduces the chances of overfitting by NN or any other machine learning classification algorithm. Functional fitting also circumvents the problem associated with flux measurements being made on an irregular time grid. Details of the function fitting are given in Sec. 3.1.

(ii) The function parameters and their associated errors obtained by fitting the analytical form to the SNe lightcurves, along with the number of flux measurements, the maximum-likelihood value of the fit and Bayesian evidence of the model are then used as input parameters to a classification NN that outputs the probability that the SN under consideration is of Type Ia. Details of NN training are given in Sec. 3.2.

### 3.1 Lightcurve fitting

All lightcurves were fitted with the following parameterised functional form, which is based on that used in Bazin et al. (2009) and Kessler et al. (2010), but differs in the precise parameterisation used:

$$f(t) = A [1 + B(t - t_1)^2] \frac{e^{-(t-t_0)/T_{\text{fall}}}}{1 + e^{-(t-t_0)/T_{\text{rise}}}}, \quad (1)$$

where, for each SN,  $t = 0$  corresponds to the time of the earliest measurement in the  $r$ -band lightcurve. While this form has no particular physical motivation, it is sufficiently general to fit the shape of virtually all types of SNe lightcurves, including those with double peaks (in contrast to the fitting function used by Newling et al. 2011). Unlike Bazin et al. (2009), we do not include an additive offset parameter, since the simulated lightcurves we will analyse have zero flux well outside the SN event by construction. One could, of course, trivially include such a parameter if, for example, one were analysing poorly-normalised real data for which this is not the case. Moreover, we use a different parameterisation for the quadratic prefactor in  $f(t)$  than that used in Kessler et al. (2010), since we feel the form we adopt in (1) has a more transparent interpretation. In particular, we restrict the parameter  $B$  to be positive, since negative values would, in general, lead to negative flux values  $f(t)$  for some ranges of  $t$ .

A separate fit was performed in each filter for each SN. To perform the fit, we assume the simple Gaussian likelihood function

$$\mathcal{L}(\Theta) = \exp[-\frac{1}{2}\chi^2(\Theta)], \quad (2)$$

where the parameter vector  $\Theta = \{A, B, t_1, t_0, T_{\text{rise}}, T_{\text{fall}}\}$  and

$$\chi^2(\Theta) = \sum_{k=1}^n \frac{[F_k - f(t_k; \Theta)]^2}{\sigma_k^2}, \quad (3)$$

in which  $n$  is the number of flux measurements for the supernova/filter combination under consideration. The priors assumed on the function parameters are listed in Table 1.

In order to estimate the function parameters, we use the `MultiNest` package (Feroz & Hobson 2008; Feroz et al. 2009) which is built on the framework of nested sampling (Skilling 2004; Sivia & Skilling 2006) and is very efficient at exploring posteriors that may contain multiple modes and/or large (curving) degeneracies, and also calculates the Bayesian log-evidence,  $\log \mathcal{Z}$ , for the model. Fig. 1 shows the data and corresponding fitted functional

Lightcurve parameter	Prior
$A$	$\mathcal{U}(10^{-5}, 1000)$ on $\log A$
$B$	$\mathcal{U}(10^{-5}, 100)$ on $\log B$
$t_1$	$\mathcal{U}(0, 100)$ MJD
$t_0$	$\mathcal{U}(0, 100)$ MJD
$T_{\text{rise}}$	$\mathcal{U}(0, 100)$ MJD
$T_{\text{fall}}$	$\mathcal{U}(0, 100)$ MJD

**Table 1.** Priors on lightcurve parameters, where  $\mathcal{U}(a, b)$  denotes a uniform distribution between the limits  $a$  and  $b$ .

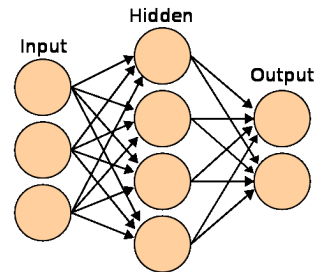


**Figure 2.** A 3-layer neural network with 3 inputs, 4 hidden nodes, and 2 outputs. Image courtesy of Wikimedia Commons.

form in each filter for a typical Type Ia and Type II SN, respectively. The function  $f(t)$  in (1) is sufficiently flexible to provide a good fit to all the lightcurves.

From each fit, the feature vector consisting of the mean values  $\hat{\Theta} = \{\hat{A}, \hat{B}, \hat{t}_1, \hat{t}_0, \hat{T}_{\text{rise}}, \hat{T}_{\text{fall}}\}$  and standard deviations  $\sigma = \{\sigma_A, \sigma_B, \sigma_{t_1}, \sigma_{t_0}, \sigma_{T_{\text{rise}}}, \sigma_{T_{\text{fall}}}\}$  of the one-dimensional marginalized posterior distributions of function parameters, along with the number of flux measurements  $n$ , the maximum-likelihood value and the Bayesian evidence, are then used as inputs for NN training. For each SN, the total input vector consists of the concatenation of the feature vectors for each filter. Since there are 15 values in the feature vector for each filter, resulting in a total of 60 values across all 4 filters, the function fitting corresponds to a dimensionality reduction relative to the number of flux measurements for some SNe, but not for others. One facet of the robustness of our approach is that the same function fitting process is performed for all SNe, irrespective of the number and times relative to peak brightness of the flux measurements in each filter. For each filter, the entire fitting process requires around 90 secs on a single CPU.

### 3.2 Neural network training

A multilayer perceptron artificial neural network is the simplest type of network and consists of ordered layers of perceptron nodes that pass scalar values from one layer to the next. The perceptron is the simplest kind of node, and maps an input vector  $\mathbf{x} \in \mathbb{R}^n$  to a scalar output  $f(\mathbf{x}; \mathbf{w}, \theta)$  via

$$f(\mathbf{x}; \mathbf{w}, \theta) = \theta + \sum_{i=1}^n w_i x_i, \quad (4)$$

where  $\{w_i\}$  and  $\theta$  are the parameters of the perceptron, called the ‘weights’ and ‘bias’, respectively. We will focus mainly on 3-layer NNs, which consist of an input layer, a hidden layer, and an output layer as shown in Fig. 2. The outputs of the nodes in the hidden and

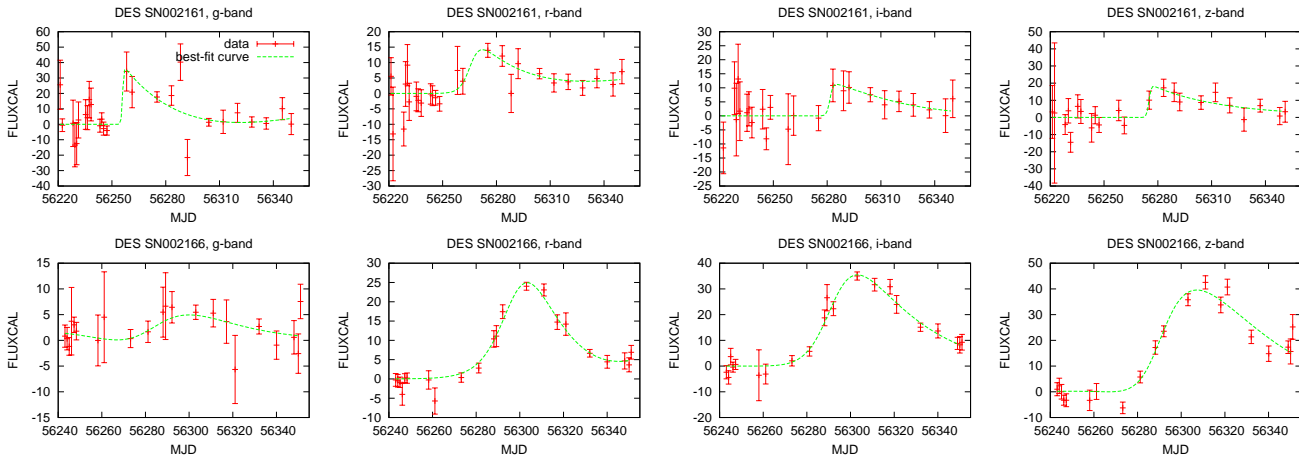


**Figure 1.** Simulated lightcurve measurements and associated uncertainties (red points) in the  $g$ ,  $r$ ,  $i$  and  $z$  filters for a Type-Ia (top row) and non-Ia (bottom row) SN, together with the best-fit function (green line) of the form in equation (1).

output layers are given by the following equations:

$$\text{hidden layer: } h_j = g^{(1)}(f_j^{(1)}); f_j^{(1)} = \theta_j^{(1)} + \sum_l w_{jl}^{(1)} x_l, \quad (5)$$

$$\text{output layer: } y_i = g^{(2)}(f_i^{(2)}); f_i^{(2)} = \theta_i^{(2)} + \sum_j w_{ij}^{(2)} h_j, \quad (6)$$

where  $l$  runs over input nodes,  $j$  runs over hidden nodes, and  $i$  runs over output nodes. The functions  $g^{(1)}$  and  $g^{(2)}$  are called activation functions and must be bounded, smooth, and monotonic for our purposes. We use  $g^{(1)}(x) = \tanh(x)$  and  $g^{(2)}(x) = x$ ; the non-linearity of  $g^{(1)}$  is essential to allowing the network to model non-linear functions.

The weights and biases are the values we wish to determine in our training. As they vary, a huge range of non-linear mappings from inputs to outputs is possible. In fact, a ‘universal approximation theorem’ (Hornik et al. 1990) states that a NN with three or more layers can approximate any continuous function as long as the activation function is locally bounded, piecewise continuous, and not a polynomial.

In order to classify a set of data using a NN, we need to provide a set of training data  $\mathcal{D} = \{\mathbf{x}^{(i)}, \mathbf{t}^{(i)}\}$ , where  $\mathbf{x}^{(i)}$  denotes the input parameters and  $\mathbf{t}^{(i)}$  is a vector with membership probabilities for each class. The likelihood function for a classification network is given by

$$\mathcal{L}(\mathbf{a}) = \sum_{i=1}^{n_t} \sum_{j=1}^{n_c} t_j^{(i)} \log p_j(\mathbf{x}^{(i)}; \mathbf{a}), \quad (7)$$

where  $n_t$  is number of training data,  $n_c$  is number of classes,  $\mathbf{a}$  denotes the network weights and biases and  $p_j$  is probability predicted by NN for class  $j$ . These probabilities are calculated using the soft-max function applied to outputs from the final layer of the NN:

$$p_j = \frac{e^{y_j}}{\sum_{j'} e^{y_{j'}}}. \quad (8)$$

Depending on the network architecture, there can be millions of network weights and biases which makes network training a very complicated and computationally challenging task. Standard methods use the gradient descent algorithm (Rumelhart et al. 1986) for network training but this does not work well for very deep networks (networks with many hidden layers). We therefore use the SkyNet

package for network training which uses a 2nd-order optimisation method based on the conjugate gradient algorithm and has been shown to train very deep networks efficiently (Feroz et al., in preparation). SkyNet has also been combined with MultiNest in the BAMB I (Graff et al. 2012) package for fast and robust Bayesian analysis.

### 3.3 Application to post-SNPCC data

In the original SNPCC, participants were given the ‘spectroscopically-confirmed’ sample  $\mathcal{S}$  and asked to predict the type of SNe in the ‘photometric’ sample  $\mathcal{P}$ . We apply our method to this case in Sec. 4, but, as we comment in Sec. 2,  $\mathcal{S}$  is not a random subset of  $\mathcal{D}$ , and so is not representative of the full data set. As discussed in Newling et al. (2011) and Richards et al. (2012), when training machine-learning methods – including neural networks – the distribution and characteristics of the training and testing samples (see below) should be as similar as possible. It can therefore cause difficulties to use  $\mathcal{S}$  for training and  $\mathcal{P}$  as the testing sample, since  $\mathcal{S}$  constitutes a biased subsample.

The original rationale for using  $\mathcal{S}$  as the training data in the SNPCC was that limited spectroscopic resources in future surveys are likely to produce a biased sample of SNe of known class. Nonetheless, studies of automated methods for photometric classification of SNe may provide sufficient motivation to modify the spectroscopic follow-up strategy (Richards et al. 2012), leading to real spectroscopically-confirmed SNe training samples that more closely represent the larger photometric sample. Therefore, following Newling et al. (2011), after deciding on the proportions of the data to be used for training and testing, we also consider partitioning  $\mathcal{D}$  randomly.

In fact, in each case, we divide the data among three different categories: optimisation, validation and testing. Data in the optimisation category constitute the  $n_t$  examples on which network weights are optimised using the likelihood function given in Eq. (7). Data in the validation category are used to guard against overfitting: when the sum of squared errors on validation data starts to increase, the network optimisation is stopped. The combination of optimisation and validation data, always in the relative proportions 75:25 per cent, constitute what we call our ‘training’ data. Data in the testing category are not involved in the training of the

network at all, and are used to assess the accuracy of the resulting classifier. All the results presented in this paper are obtained from the testing data-set.

It is interesting to check the improvement in network predictions with the amount of data used in training, we therefore construct six random training samples  $\mathcal{D}_p$  ( $p = 0, 1, 2, \dots, 5$ ), which contain 5, 10, 20, 30, 40 and 50 per cent of the data, respectively, and the use remainder of the data for testing. Sample  $\mathcal{D}_0$  contains 1045 SNe and is thus similar in size to the spectroscopically-confirmed sample  $\mathcal{S}$  discussed above. Clearly, as the amount of data used for training increases, one should expect the accuracies of predictions coming from networks to improve.

For each sample, we use the following input set for network training:  $\mathbf{x}^{(i)} = \{\hat{\Theta}_i^\alpha, \hat{\sigma}_i^\alpha, n_i^\alpha, (\log \mathcal{L}_{\max})_i^\alpha, \log \mathcal{Z}_i^\alpha\}$ , where  $i$  indexes the SNe allocated to a given optimisation, validation and testing category,  $\alpha \in \{g, r, i, z\}$  denotes the filter,  $\hat{\Theta}_i^\alpha$  and  $\hat{\sigma}_i^\alpha$  are the means and standard deviations respectively of function parameters defined in Sec. 3.1,  $n_i^\alpha$  is the number of flux measurements for a given SN,  $(\log \mathcal{L}_{\max})_i^\alpha$  is the maximum-likelihood value of the fit and  $\log \mathcal{Z}_i^\alpha$  is the Bayesian log-evidence. Moreover, we also train further networks with redshift  $z_i$  and its uncertainty  $\sigma_{z_i}$  included as additional inputs, in order to determine whether they can improve the SNe classification.

We use a 3-layered perceptron neural network with 500 nodes in the hidden layer. Training times on 16 processors for datasets  $\mathcal{D}_0$  and  $\mathcal{D}_5$  (i.e. the smallest and largest of those considered), including redshift information, were  $\sim 2$  and  $\sim 52$  min, respectively.

## 4 RESULTS

Once the network has been trained, it is applied to the testing data-set to obtain the predictions for each SN therein being either Type-Ia or non-Ia. For each SN, the NN classification requires only a few microseconds of CPU time. To perform the classification, we first need to pick a threshold probability  $p_{\text{th}}$  such that all SNe for which the network output probability of being Type-Ia is larger than  $p_{\text{th}}$  are identified as Type-Ia candidates. One can then calculate the completeness  $\epsilon_{\text{Ia}}$  (fraction of all type Ia SNe that have been correctly classified; also often called the efficiency), purity  $\tau_{\text{Ia}}$  (fraction of all Type Ia candidates that have been classified correctly) and figure of merit  $\mathcal{F}_{\text{Ia}}$  for Type Ia SNe. These quantities are defined as follows:

$$\epsilon_{\text{Ia}} = \frac{N_{\text{Ia}}^{\text{true}}}{N_{\text{Ia}}^{\text{total}}}, \quad (9)$$

$$\tau_{\text{Ia}} = \frac{N_{\text{Ia}}^{\text{true}}}{N_{\text{Ia}}^{\text{true}} + N_{\text{Ia}}^{\text{false}}}, \quad (10)$$

$$\mathcal{F}_{\text{Ia}} = \frac{1}{N_{\text{Ia}}^{\text{total}}} \frac{(N_{\text{Ia}}^{\text{true}})^2}{N_{\text{Ia}}^{\text{true}} + W N_{\text{Ia}}^{\text{false}}}, \quad (11)$$

where  $N_{\text{Ia}}^{\text{total}}$  is the total number of Type Ia SNe in the sample,  $N_{\text{Ia}}^{\text{true}}$  is the number of SNe correctly predicted to be of Type Ia,  $N_{\text{Ia}}^{\text{false}}$  is the number of SNe incorrectly predicted to be of Type Ia and  $W$  is a penalty factor which controls the relative penalty for false positives over false negatives. For SNPCC  $W \equiv 3$ .

Our classification results using a canonical threshold probability  $p_{\text{th}} = 0.5$  are summarised in Table 2. It can be clearly seen that there is a significant improvement in the results as more training data are used. Moreover, comparing the results for training samples  $\mathcal{S}$  and  $\mathcal{D}_0$ , which are similar in size, one sees that the overall quality of the classification is much higher for the random, representative

Sample	$z$ used	Completeness	Purity	FoM
$\mathcal{S}$	no	0.93	0.32	0.12
$\mathcal{D}_0$	no	0.71	0.67	0.29
$\mathcal{D}_1$	no	0.78	0.77	0.41
$\mathcal{D}_2$	no	0.79	0.79	0.43
$\mathcal{D}_3$	no	0.82	0.80	0.46
$\mathcal{D}_4$	no	0.82	0.82	0.50
$\mathcal{D}_5$	no	0.85	0.82	0.51
$\mathcal{S}$	yes	0.94	0.34	0.14
$\mathcal{D}_0$	yes	0.75	0.70	0.33
$\mathcal{D}_1$	yes	0.79	0.78	0.43
$\mathcal{D}_2$	yes	0.82	0.81	0.48
$\mathcal{D}_3$	yes	0.84	0.83	0.52
$\mathcal{D}_4$	yes	0.84	0.85	0.55
$\mathcal{D}_5$	yes	0.88	0.85	0.58

**Table 2.** Completeness, purity and figure of merit for Type-Ia SNe classification obtained by applying trained networks to the various testing data-sets with threshold probability  $p_{\text{th}}$  set to 0.5.

sample  $\mathcal{D}_0$  than for the biased sample  $\mathcal{S}$ ; this agrees with the findings of Newling et al. (2011) and Richards et al. (2012). Nonetheless, although the purity obtained for the sample  $\mathcal{S}$  is quite low, the completeness is very high. This is most likely because of the biased nature of  $\mathcal{S}$ , in which about 51 per cent of SNe are Type-Ia, whereas  $\mathcal{P}$  contains only 22 per cent Type-Ia. Thus, the classifier has not been trained with a representative collection of non-Ia SNe, and hence often misclassifies them as Type-Ia. It is worth noting that the ‘toy classifier’, which simply classifies all SNe in  $\mathcal{P}$  as Type Ia, would yield  $\epsilon_{\text{Ia}} = 1.00$ ,  $\tau_{\text{Ia}} = 0.22$  and  $\mathcal{F}_{\text{Ia}} = 0.09$ .

The inclusion of redshift information results in a modest 5–10 per cent improvement in  $\epsilon_{\text{Ia}}$ ,  $\tau_{\text{Ia}}$  and  $\mathcal{F}_{\text{Ia}}$  for each random sample  $\mathcal{D}_p$ , but only a very marginal improvement for  $\mathcal{S}$ . In Fig. 3 we show the completeness, purity and figure of merit for Type Ia classification as function of SNe redshift  $z$  for the training samples  $\mathcal{D}_1$  and  $\mathcal{D}_4$ . One sees that the completeness (efficiency) shows no dependence on  $z$ , but that there is a slight drop-off in purity (and hence FoM) at low  $z$ . This probably occurs because the percentage of Type Ia SN is lower at low redshift, which would indeed be expected to reduce purity, but not completeness. This is most easily understood by again considering the ‘toy classifier’ mentioned above, which would clearly display this behaviour; we would expect facets of this generic behaviour to occur for any classification method.

An important feature of probabilistic classification is that it allows one to investigate the quality of the classification as a function of the threshold probability. Moreover, as pointed out in Feroz et al. (2008), it also allows one to calculate the *expected* completeness, purity and figure of merit as a function of  $p_{\text{th}}$ , *without* knowing the true classes of the SNe in the testing sample (as is the case in classification of real SNe data, in the absence of spectroscopic follow-up observations). Equally, these expected values can be calculated without the need to perform an average explicitly over realisations of the testing sample.

Let us assume that the predicted probabilities for each SN being of Type Ia are given by  $p_{\text{Ia},i}$ . The expected values of the total number  $\hat{N}_{\text{Ia}}^{\text{total}}$  of Type Ia SNe in the sample, the number  $\hat{N}_{\text{Ia}}^{\text{true}}$  of SNe correctly predicted to be of Type Ia, and the number  $\hat{N}_{\text{Ia}}^{\text{false}}$  of SNe incorrectly predicted to be of Type Ia can then be calculated

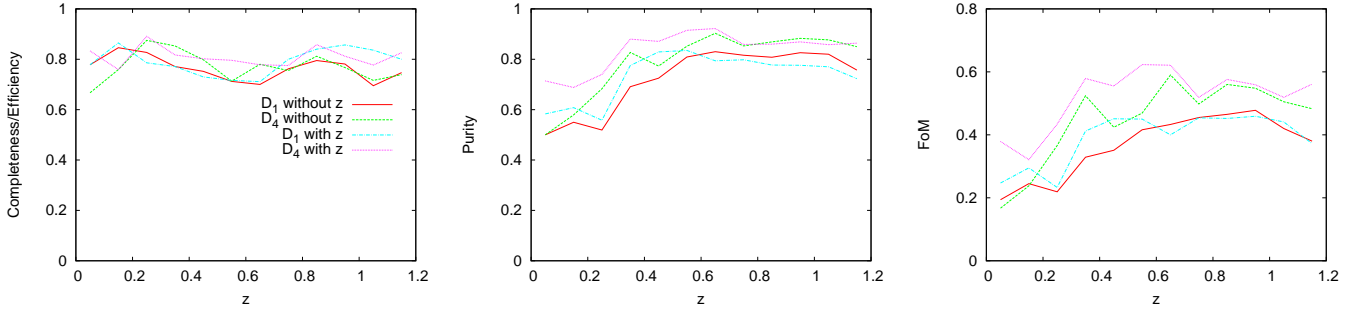


**Figure 3.** Completeness, purity and figure of merit for Type-Ia SNe classification as a function of redshift ( $z$ ) from applying trained networks with a threshold probability ( $p_{\text{th}}$ ) of 0.5; ‘with  $z$ ’/‘without  $z$ ’ indicates that redshift information was/was not used in network training. Samples  $\mathcal{D}_1$  and  $\mathcal{D}_4$  use 10 and 40 per cent of the data, respectively, for training.

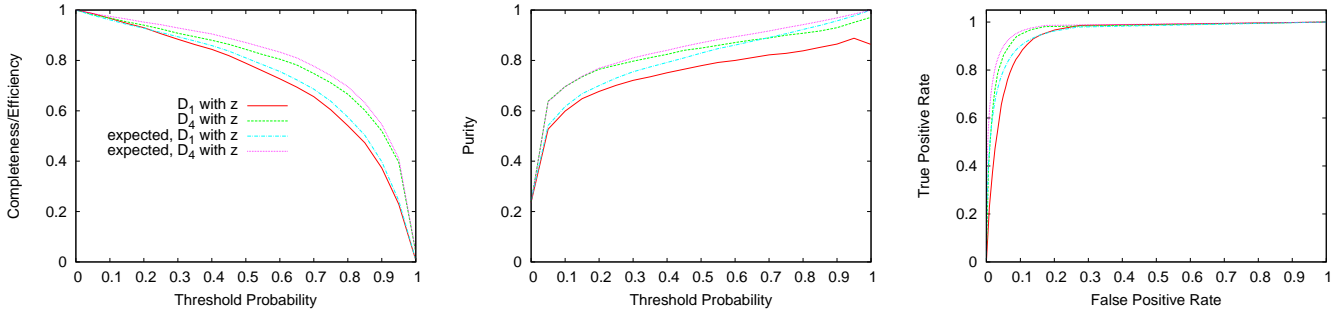


**Figure 4.** True and expected completeness, purity and Receiver Operating Characteristic (ROC) as a function of threshold probability  $p_{\text{th}}$  from applying trained networks to get Ia/non-Ia classification probabilities on the testing data-set. No redshift information was used in network training. Samples  $\mathcal{D}_1$  and  $\mathcal{D}_4$  use 10 and 40 per cent of the data, respectively, for training.

as follows:

$$\hat{N}_{\text{Ia}}^{\text{total}} = \sum_{i=1}^N p_{\text{Ia},i}, \quad (12)$$

$$\hat{N}_{\text{Ia}}^{\text{true}} = \sum_{i=1, p_{\text{Ia},i} > p_{\text{th}}}^N p_{\text{Ia},i}, \quad (13)$$

$$\hat{N}_{\text{Ia}}^{\text{false}} = \sum_{i=1, p_{\text{Ia},i} > p_{\text{th}}}^N 1 - p_{\text{Ia},i}, \quad (14)$$

where  $N$  is the total number of SNe classified and  $p_{\text{th}}$  is the threshold probability. We can then use Eqs. (10), (11) and (11) to calculate the expected values of completeness  $\hat{\epsilon}_{\text{Ia}}$ , purity  $\hat{\tau}_{\text{Ia}}$  and figure of merit  $\hat{\mathcal{F}}_{\text{Ia}}$  as a function of threshold probability  $p_{\text{th}}$ .

In Fig. 4, we plot the actual and expected values of completeness and purity for the samples  $\mathcal{D}_1$  and  $\mathcal{D}_4$ , trained without redshift information. Plots for networks trained with redshift information are quite similar and therefore we do not show them. One sees that the expected completeness and purity curves match quite well with the corresponding actual ones. Thus, in principle, rather than arbitrarily choosing the value  $p_{\text{th}} = 0.5$  (say), which was used to produce the results in Table 2 and Fig. 3, one could instead choose a value of  $p_{\text{th}}$  designed to achieve a target overall completeness and/or purity for a given survey.

We also plot the actual and expected Receiver Operating Characteristic (ROC) curves (see e.g. Fawcett 2006) for our analysis procedure in Fig. 4. The ROC curve provides a very reliable way

of selecting the optimal algorithm in signal detection theory. We employ the ROC curve here to analyse our SNe classification criterion, based on the threshold probability  $p_{\text{th}}$ . The ROC curve plots the True Positive Rate (TPR) against the False Positive Rate (FPR) as a function of the threshold probability. TPR is, in fact, identical to completeness (and also equals the ‘power’ of the classification test in a Neyman–Pearson sense); it may also be defined as the ratio of the number of true positives for a given  $p_{\text{th}}$  to the number of true positives for  $p_{\text{th}} = 0$ . Conversely, FPR is the ratio of the number of false positives for a given  $p_{\text{th}}$  to the number of false positives for  $p_{\text{th}} = 0$ , which is also often referred to as the contamination (or the Neyman–Pearson type-I error rate)<sup>1</sup>. A perfect binary classification method would yield a ROC curve in the form of a right-angle connecting the points (0, 0) and (1, 0) in the ROC space via the upper left corner (0, 1). A completely random classifier would yield a diagonal line connecting (0, 0) and (1, 0) directly.

One sees from the right-hand panel in Fig. 4 that our method yields very reasonable ROC curves, indicating that the classifiers are quite discriminative. One also sees that our expected ROC curves match well with the corresponding actual ones. Thus, in principle, one could ‘optimise’ the classifier by choosing  $p_{\text{th}}$  in a number of possible ways. For example, from among the numerous possibilities, one could choose  $p_{\text{th}}$  such that it corresponds to the

<sup>1</sup> It is worth noting that, in terms of conditional probabilities, completeness is simply  $\Pr(\text{classified as Ia}|\text{Ia})$ , purity is its Bayes’ theorem complement  $\Pr(\text{Ia}|\text{classified as Ia})$ , and contamination is  $\Pr(\text{classified as Ia}|\text{non-Ia})$ .



point on the expected ROC curve where, either: (i) the ROC curve crosses the straight line connecting the (0, 1) and (1, 0) in the ROC space; or (ii) the straight line joining the point (1, 0) to the ROC curve intersects it at right-angles.

## 5 DISCUSSION AND CONCLUSIONS

We have presented a new method for performing automated photometric of SNe into Type-Ia and non-Ia. In our a two-stage approach, the SNe lightcurves are first fitted to an analytic parameterised function, and the resulting parameters, together with a few further statistics associated with the fit, are then used as the input feature vector to a classification neural network whose output is the probability that the SN is of Type-Ia. Assuming a canonical threshold output probability  $p_{\text{th}} = 0.5$ , when we train the method using a random sample of 10 (40) per cent of the updated simulated data set released following the SuperNova Photometric Classification Challenge (post-SNPCC), making no selection cuts, we find that it yields robust classification results, namely a completeness of 0.78 (0.82), purity of 0.77 (0.82), and SNPCC figure-of-merit of 0.41 (0.50). A modest 5–10 per cent improvement in these results is achieved by also including the SN host-galaxy redshift and its uncertainty as inputs to the classification network. The quality of the classification does not depend strongly on the SN redshift.

It is difficult to perform a direct comparison of our results with those submitted to the original SuperNova Photometric Classification Challenge, which are summarised in Kessler et al. (2010). As pointed out in that paper, the original challenge data set suffered from a number of bugs; these were subsequently corrected before the release of the post-SNPCC data set used in this paper. The latter also benefited from further improvement in the generation of the simulations, leading to more realistic SNe lightcurves. It is hard to assess how these differences affect the difficulty of classifying the SNe. For example, in the original SNPCC data set, non-Ia SNe were too dim on average, which made classification of Type-Ia SNe easier. Conversely, participants in the original SNPCC were given the spectroscopically confirmed sample  $\mathcal{S}$  of 1,103 SNe and asked to predict the type of SNe in the simulated sample  $\mathcal{P}$  of 20,216 SNe. As discussed in Sec. 2, the fact that  $\mathcal{S}$  is not a representative training sample makes classification more difficult than if one simply uses random training samples, on which most of our analysis has been focused. Despite these caveats, for reference we note that the original challenge entry with the highest SNPCC figure of merit of  $\sim 0.4$  (averaged over SN redshift bins), achieved an overall completeness of 0.96 and purity of 0.79, although the quality of the classification varied considerably with SN redshift.

More recent works by Newling et al. (2011), Richards et al. (2012) and Ishida & de Souza (2012) analyse the same post-SNPCC data set  $\mathcal{D}$  used in this paper. A meaningful comparison of their results with our own is still not straightforward, however, since all three studies make different choices for the nature and size of the subsets of  $\mathcal{D}$  used for training and testing, which also differ from the choices made in this paper. Nonetheless, some broad comparisons are possible.

The most straightforward comparison is with Newling et al. (2011), who present results using, as we do, the subset  $\mathcal{S}$  and also various random subsets of  $\mathcal{D}$  (which they call ‘representative samples’) for training their classifier. For  $\mathcal{S}$ , their KDE method achieves a figure-of-merit of 0.37 (0.39) without (with) the inclusion of host-galaxy redshift information, whereas their boosting method yields a figure-of merit of 0.15 using redshift information. Turning to their

analysis of representative samples, from figure 15 in their paper, one sees that their boosting method, which is the more successful of their two methods on the representative samples, achieves figures-of-merit of  $\sim 0.45$  and  $\sim 0.55$  for training sets containing  $\sim 2000$  and  $\sim 8000$  SNe, respectively, which correspond roughly to the sizes of our  $\mathcal{D}_1$  and  $\mathcal{D}_4$  training data sets. These classification results are obtained from the remaining SNe in  $\mathcal{D}$ , after including SNe host-galaxy redshift information, and are very similar to the equivalent figures-of-merit achieved by our own classifier, as listed in Table 2. Unfortunately, Newling et al. (2011) do not give values for their corresponding completeness and purity values, so it is not possible to compare their results with our own.

Both Richards et al. (2012) and Ishida & de Souza (2012) adopt very different approaches from the above, and from each other, for choosing the nature and size of the subsets of  $\mathcal{D}$  used for training. Indeed, each of these works considers a range of training sets. Richards et al. (2012) do, however, consider training using the spectroscopically-confirmed sample  $\mathcal{S}$ , and obtain a purity of 0.50 (0.54), a completeness of 0.50 (0.90) and a figure-of-merit of 0.13 (0.25) without (with) the inclusion of redshift information. They also construct three further classes of training sets, two of which contain several examples, each requiring the same fixed amount of spectroscopic follow-up time assumed in the construction of the original sample  $\mathcal{S}$ . These are: (i) SNe observed in order of decreasing brightness; (ii) ( $r$  band) magnitude-limited surveys down to 23.5, 24. 24.5 and 25th magnitude, respectively; and (iii) redshift-limited surveys out to  $z = 0.4$  and 0.6, respectively. In applying their classifier to the post-SNPCC the remaining part of the photometric sample  $\mathcal{P}$ , their best classification results are a completeness of 0.65 (0.74), a purity of 0.72 (0.76) and a figure-of-merit of 0.31 (0.36) without (with) the inclusion of redshift information; these were obtained from the deepest magnitude-limited survey, which contained only 165 SNe. It is worth noting the deeper training sets have a SNe class composition that closely resembles that of the full data set  $\mathcal{D}$ , and so begin to approximate a representative training sample.

The training sets considered by Ishida & de Souza (2012) are closer in spirit to the one used in the original SNPCC. Starting with the spectroscopically-confirmed subsample  $\mathcal{S}$ , as a requirement of their method they impose selection cuts such that every SN must have at least one observation epoch with  $t \leq t_{\text{low}}$  and one with  $t \geq t_{\text{up}}$  in all available filters. In addition, each SN must have at least 3 observations above a given signal-to-noise ratio (SNR) in each filter. The same selection cuts are also applied to the photometric subsample  $\mathcal{P}$  to produce the corresponding testing sets. Of the selection cuts considered, their sample  $\mathcal{D}_5$  with  $\text{SNR} > 0$  is the least restrictive, yielding training and testing sets containing 830 and 15,988 SNe, respectively. On these demanding data their classifier yields a completeness of 0.44, a purity of 0.37, and a figure-of-merit of 0.06.

From these various comparisons, we conclude that the method presented in this paper is indeed competitive, in spite of its relative simplicity, and yields reasonably robust classifications. Finally, we note that, aside from its relative simplicity and robustness, the classification method that we have presented here can be extended and improved in a number of ways. Firstly, one can easily generalise our approach to divide the non-Ia SNe into their different classes. Moreover, our use of probabilistic classification allows one to calculate expected completeness, purity and figure-of-merit (amongst other measures), without knowing the true classes of the SNe in the testing sample, as will be the case in the classification of real SNe. This allows one to tailor the method by adjusting the output

threshold probability  $p_{th}$  to achieve a given completeness, purity or figure-of-merit. Alternatively, one could use the expected ROC curve to optimise the value of  $p_{th}$  used for classification. Nonetheless, one must always remember that if the training sample is not representative of the population, then the predictions for any measure of classification quality will inevitably be biased, in which case the derived threshold probability may, in fact, not be optimal. We plan to investigate these issues in a future work.

## ACKNOWLEDGEMENTS

We thank Marisa March for many insightful discussions regarding supernovae astronomy, and the two referees for their valuable suggestions. NVK thanks Ariel Goobar for his critical, but simultaneously motivating, comments regarding our classification method, and Johannes Bergstrom and Chris Savage for useful comments at an early stage of the analysis. NVK also acknowledges support from the Swedish Research Council (contract No. 621-2010-3301). FF is supported by a Research Fellowship from Trinity Hall, Cambridge. This work was performed primarily on COSMOS VIII, an SGI Altix UV1000 supercomputer, funded by SGI/Intel, HEFCE and PPARC. The work also utilized the Darwin Supercomputer of the University of Cambridge High Performance Computing Service (<http://www.hpc.cam.ac.uk>), provided by Dell Inc. using Strategic Research Infrastructure Funding from the Higher Education Funding Council for England.

## REFERENCES

- Annis J. T., Cunha C., Busha M., Ma Z., DES Collaboration 2011, in American Astronomical Society Meeting Abstracts 217 Vol. 43 of Bulletin of the American Astronomical Society, The Dark Energy Survey: Survey Strategy. p. 433.16
- Bazin G., et al., 2009, *A&A*, 499, 653
- Benitez-Herrera S., Röpke F., Hillebrandt W., Mignone C., Bartelmann M., Weller J., 2012, *MNRAS*, 419, 513
- Blake C., et al., 2011, *MNRAS*, 418, 1707
- Conley A., et al., 2011, *ApJS*, 192, 1
- D’Andrea C. B., et al., 2010, *ApJ*, 708, 661
- Dodelson S., Vallinotto A., 2006, *Phys.Rev.D*, 74, 063515
- Falck B. L., Riess A. G., Hlozek R., 2010, *ApJ*, 723, 398
- Fawcett T., 2006, *Pattern Recogn. Lett.*, 27, 861
- Feroz F., Hobson M. P., 2008, *MNRAS*, 384, 449
- Feroz F., Hobson M. P., Bridges M., 2009, *MNRAS*, 398, 1601
- Feroz F., Marshall P. J., Hobson M. P., 2008, *ArXiv e-prints*
- Fryer C. L., et al., 2007, *PASP*, 119, 1211
- Gong Y., Cooray A., Chen X., 2010, *ApJ*, 709, 1420
- Graff P., Feroz F., Hobson M. P., Lasenby A., 2012, *MNRAS*, 421, 169
- Hillebrandt W., Niemeyer J. C., 2000, *ARA&A*, 38, 191
- Homeier N. L., 2005, *ApJ*, 620, 12
- Hornik K., Stinchcombe M., White H., 1990, *Neural Networks*, 3, 359
- Ishida E. E. O., de Souza R. S., 2012, *ArXiv e-prints*
- Ivezic Z., et al., 2008, *ArXiv e-prints*
- Johnson B. D., Crotts A. P. S., 2006, *AJ*, 132, 756
- Jönsson J., Dahlén T., Goobar A., Mörtzell E., Riess A., 2007, *JCAP*, 6, 2
- Jönsson J., Dahlén T., Hook I., Goobar A., Mörtzell E., 2010a, *MNRAS*, 402, 526
- Jönsson J., Sullivan M., Hook I., Basa S., Carlberg R., Conley A., Fouchez D., Howell D. A., Perrett K., Pritchett C., 2010b, *MNRAS*, 405, 535
- Karpenka N. V., March M. C., Feroz F., Hobson M. P., 2012, *ArXiv e-prints*
- Kessler R., et al., 2009, *ApJS*, 185, 32
- Kessler R., et al., 2009, *arXiv:0908.4280*
- Kessler R., et al., 2010, *PASP*, 122, 1415
- Kronborg T., et al., 2010, *A&A*, 514, A44
- Kunz M., Bassett B. A., Hlozek R. A., 2007, *Phys.Rev.D*, 75, 103508
- Kuznetsova N. V., Connolly B. M., 2007, *ApJ*, 659, 530
- Mantz A., Allen S. W., Rapetti D., Ebeling H., 2010, *MNRAS*, 406, 1759
- March M. C., Trotta R., Berkes P., Starkman G. D., Vaudrevange P. M., 2011, *MNRAS*, 418, 2308
- Metcalf R. B., 1999, *MNRAS*, 305, 746
- Metcalf R. B., Silk J., 1999, *ApJ*, 519, L1
- Newling J., Varughese M., Bassett B., Campbell H., Hlozek R., Kunz M., Lampeitl H., Martin B., Nichol R., Parkinson D., Smith M., 2011, *MNRAS*, 414, 1987
- Nugent P., Kim A., Perlmutter S., 2002, *PASP*, 114, 803
- Perlmutter S., et al., 1999, *ApJ*, 517, 565
- Poznanski D., Gal-Yam A., Maoz D., Filippenko A. V., Leonard D. C., Matheson T., 2002, *PASP*, 114, 833
- Poznanski D., Maoz D., Gal-Yam A., 2007, *AJ*, 134, 1285
- Rauch K. P., 1991, *ApJ*, 374, 83
- Richards J. W., Homrighausen D., Freeman P. E., Schafer C. M., Poznanski D., 2012, *MNRAS*, 419, 1121
- Riess A. G., et al., 1998, *AJ*, 116, 1009
- Rodney S. A., Tonry J. L., 2009, *ApJ*, 707, 1064
- Rumelhart D. E., Hinton G. E., Williams R. J., 1986, MIT Press, Cambridge, MA, USA, Chapt. Learning internal representations by error propagation, pp 318–362
- Sako M., Bassett B., Connolly B., Dilday B., Cambell H., Frieman J. A., Gladney L., Kessler R., Lampeitl H., Marriner J., Miquel R., Nichol R. C., Schneider D. P., Smith M., Sollerman J., 2011, *ApJ*, 738, 162
- Sako M., et al., 2008, *AJ*, 135, 348
- Schmidt B. P., Keller S. C., Francis P. J., Bessell M. S., 2005, in American Astronomical Society Meeting Abstracts #206 Vol. 37 of Bulletin of the American Astronomical Society, The SkyMapper Telescope and Southern Sky Survey. p. 457
- Sivia D., Skilling J., 2006, *Data Analysis A Bayesian Tutorial*. Oxford University Press
- Skilling J., 2004, in Fischer R., Preuss R., Toussaint U. V., eds, American Institute of Physics Conference Series Vol. 119, Nested Sampling. pp 1211–1232
- Sullivan M., et al., 2006, *AJ*, 131, 960
- Sullivan M., et al., 2011, *ApJ*, 737, 102
- Tyson J. A., 2002, in Tyson J. A., Wolff S., eds, Society of Photo-Optical Instrumentation Engineers (SPIE) Conference Series Vol. 4836 of Society of Photo-Optical Instrumentation Engineers (SPIE) Conference Series, Large Synoptic Survey Telescope: Overview. pp 10–20
- Wester W., Dark Energy Survey Collaboration 2005, in Wolff S. C., Lauer T. R., eds, Observing Dark Energy Vol. 339 of Astronomical Society of the Pacific Conference Series, Dark Energy Survey and Camera. p. 152
- Zentner A. R., Bhattacharya S., 2009, *ApJ*, 693, 1543